

# An empirical study of hydrocarbon indicators

Brian Russell<sup>1</sup>, Hong Feng, and John Bancroft

<sup>1</sup> Hampson-Russell, A CGGVeritas Company, Calgary, Alberta, [brian.russell@cggveritas.com](mailto:brian.russell@cggveritas.com)

## ABSTRACT

Numerous approaches have been published that derive fluid indicators, often called direct hydrocarbon indicators (DHI), from the amplitude variations with offset (AVO) method. These methods use linearized approximations to the Zoeppritz equations to extract physical parameters such as  $P$ -impedance,  $S$ -impedance, density, bulk modulus, shear modulus, Lamé's parameters and Poisson's ratio, and then infer the fluid content of a hydrocarbon reservoir from these parameters. Russell et al. (2003) used poroelasticity theory (Biot, 1941) to generalize several of these methods using a parameter dependent on the dry rock  $V_P/V_S$  ratio. The purpose of this study is to examine the generalized fluid method and compare this method with other fluid methods to see which indicator can most effectively discriminate between hydrocarbon sands and wet sands and which indicator is most sensitive to pore-fluid content estimation. To perform the sensitivity analysis we use an empirical dataset measured by Han et al. (1985), which covers saturated and dry sands with a wide range of porosities and clay contents at different pressures. As an indicator to evaluate the best method, we use the measure suggested by Dillon et al. (2003) in their analysis of fluid indicators. Using Han's dataset, we conclude that the generalized fluid method is in general the most successful fluid discriminant, given that we can get a reliable estimate of the dry rock  $V_P$  to  $V_S$  ratio. We are also able to make predictions about the dry rock  $V_P$  to  $V_S$  ratio as a function of porosity, clay content and pressure, which is related to depth.

## INTRODUCTION

Traditional seismic data interpretation was performed to identify structural traps where hydrocarbons had potentially accumulated. Later, bright-spot technology was used to identify amplitude anomalies on stacked data that would indicate a gas accumulation. Most recently, pre-stack seismic data has been analyzed to look for hydrocarbon anomalies, using both amplitude variations with offset (AVO) reflectivity analysis and pre-stack inversion. Using the attributes derived from AVO and pre-stack inversion, many other indicators have been used or proposed, such as the fluid factor (Fatti et al., 2003), the lambda-mu-rho (LMR) method (Goodway et al., 1997), and the generalized fluid method (Russell, 2003). The result of this is a vast array of seismic tools available to the modern seismic interpreter. However, which tool will produce the best results is often difficult to determine, since most authors focus on their particular method, and even when the methods are compared the data used is real data for which the correct answer is difficult to determine. The objectives of this study are therefore to:

1. Summarize the various fluid discrimination methods and compare them with each other, and

2. Use various a well calibrated set of core measurements to study the sensitivity of each discriminator to the fluid content.

The laboratory data used was measured by Han et al. (1985) and covers a wide range of porosities and clay contents at different pressures for both the dry and saturated cases. These samples are used not only for calculating the fluid terms but also for investigating the effect of clay content, porosity, and pressure, and for finding the squared dry rock velocity ratio  $(V_p/V_p)_{dry}^2$  in sandstone, which is needed for the correct implementation of the generalized fluid method.

It is felt that by using laboratory measurements we will arrive at a better understanding of the strengths of the various methods.

### LINEARIZED AVO APPROXIMATIONS

It has been shown (Aki and Richards, 2002) that, for small changes in the  $P$ -wave velocity,  $S$ -wave velocity and density across a boundary between two elastic media, the  $P$ -wave reflection coefficient for an incident  $P$ -wave as a function of angle can be approximated by the following linearized sum of three terms:

$$R_{PP}(\theta) = (1 + \tan^2 \theta) \frac{\Delta V_p}{2V_p} + \left[ \frac{-8 \sin^2 \theta}{\gamma_{sat}^2} \right] \frac{\Delta V_s}{2V_s} + \left[ 1 - \frac{\sin^2 \theta}{\gamma_{sat}^2} \right] \frac{\Delta \rho}{2\rho}, \quad (1)$$

where  $V_p$ ,  $V_s$  and  $\rho$  are the average velocity and density values across the boundary,  $\Delta V_p$ ,  $\Delta V_s$  and  $\Delta \rho$  are the differences of the velocity and density values across the boundary,  $\theta$  is the average of the incident and refracted angles, and  $\gamma_{sat} = V_p/V_s$  for the in-situ (saturated) rocks. By “small” changes, we mean that equation (1) is valid where each ratio  $\Delta p/p$  (which we refer to as “reflectivity” terms) is less than approximately 0.1. If we know the relationship between offset and angle for a seismic CMP gather, equation (1) can be used to extract estimates of the three reflectivities  $\frac{\Delta V_p}{2V_p}$ ,  $\frac{\Delta V_s}{2V_s}$  and  $\frac{\Delta \rho}{2\rho}$  from seismic gathers using a weighted least-squares approach.

There are several important algebraic re-arrangements of equation (1). First, it can be transformed into the three term sum given by

$$R_{PP}(\theta) = A + B \sin^2 \theta + C \tan^2 \theta \sin^2 \theta, \quad (2)$$

where  $A = R_{P0} = \frac{1}{2} \left[ \frac{\Delta V_p}{V_p} + \frac{\Delta \rho}{\rho} \right]$  is a linearized approximation to the zero-offset  $P$ -wave reflection coefficient,  $B = \frac{\Delta V_p}{2V_p} - \frac{4}{\gamma_{sat}^2} \frac{\Delta V_s}{V_s} - \frac{2}{\gamma_{sat}^2} \frac{\Delta \rho}{\rho}$ , and  $C = \frac{\Delta V_p}{2V_p}$ .

This equation (Shuey, 1985) is the basis of much of the empirical amplitude variations with offset (AVO) work performed today and has the advantage that an estimate of  $\gamma_{sat}$  is not needed in the weighting coefficients used to extract the three parameters  $A$ ,  $B$  and  $C$  (generally called the intercept, gradient, and curvature terms).

A second re-arrangement of equation (1), by Fatti et al. (1994), is given by

$$R_{PP}(\theta) = [1 + \tan^2 \theta] R_{P0} + \left[ \frac{-8}{\gamma_{sat}^2} \sin^2 \theta \right] R_{S0} + \left[ \frac{\sin^2 \theta}{\gamma_{sat}^2} - \tan^2 \theta \right] R_D, \quad (3)$$

where  $R_{P0}$  is equal to the  $A$  term from equation (2),  $R_{S0} = \left[ \frac{\Delta V_s}{V_s} + \frac{\Delta \rho}{\rho} \right]$  is a linearized approximation to the S-wave reflectivity, and  $R_D = \frac{\Delta \rho}{2\rho}$  is the linearized density reflectivity term from equation (1). Equation (3) has been used both to extract the reflectivity terms from a CMP gather and as the basis for impedance inversion (Hampson et al., 2006), and differs from equation (2) in that it requires an estimate of  $\gamma_{sat}$  in the weighting coefficients. The key fluid indicator that is derived from equation (3) is the fluid factor, which can be written:

$$\Delta F = R_{P0} - 1.16 \frac{V_s}{V_p} R_{S0}$$

Another way of re-formulating equation (1) involves transforming to parameters which are nonlinearly related to velocity and density. This involves the use of differentials as well as algebra. For example, Shuey (1982) transformed the second term in equation (2) to from dependence on  $V_s$  and  $\Delta V_s$  to dependence on Poisson's ratio  $\sigma = (\gamma - 2)/(2\gamma - 2)$  and changes in Poisson's ratio ( $\Delta\sigma$ ). Shuey's gradient term  $B$  is written

$$B = A \left[ D - 2(1+D) \frac{1-2\sigma}{1-\sigma} \right] + \frac{\Delta\sigma}{(1-\sigma)^2}, \quad (5)$$

where  $D = \frac{\Delta V_p / V_p}{\Delta V_p / V_p + \Delta \rho / \rho} = \frac{\Delta V_p / V_p}{2A}$ ,  $\sigma = \frac{\sigma_2 + \sigma_1}{2}$ ,  $\Delta\sigma = \sigma_2 - \sigma_1$ .

More recently, Gray et al. (1999) re-formulated equation (1) for two sets of fundamental constants:  $\lambda$ ,  $\mu$  and  $\rho$ , and  $K$ ,  $\mu$  and  $\rho$ , where we recall the following relationships:

$$V_p = \sqrt{\frac{\lambda + 2\mu}{\rho}} = \sqrt{\frac{K + \frac{4}{3}\mu}{\rho}}, \quad (6)$$

and

$$V_s = \sqrt{\frac{\mu}{\rho}} . \quad (7)$$

As with Shuey's work, this re-formulation required the use of both algebra and differentials relating  $\lambda$ ,  $\mu$  and  $K$  to  $V_p$ ,  $V_s$  and  $\rho$ . Gray et al.'s two formulations are given as

$$R_{pp}(\theta) = \left( \frac{1}{4} - \frac{1}{2\gamma_{sat}^2} \right) \sec^2 \theta \frac{\Delta\lambda}{\lambda} + \frac{1}{\gamma_{sat}^2} \left( \frac{1}{2} \sec^2 \theta - 2 \sin^2 \theta \right) \frac{\Delta\mu}{\mu} + \left( \frac{1}{2} - \frac{1}{4} \sec^2 \theta \right) \frac{\Delta\rho}{\rho} , \quad (8)$$

and

$$R_{pp}(\theta) = \left( \frac{1}{4} - \frac{1}{3\gamma_{sat}^2} \right) \sec^2 \theta \frac{\Delta K}{K} + \frac{1}{\gamma_{sat}^2} \left( \frac{1}{3} \sec^2 \theta - 2 \sin^2 \theta \right) \frac{\Delta\mu}{\mu} + \left( \frac{1}{2} - \frac{1}{4} \sec^2 \theta \right) \frac{\Delta\rho}{\rho} . \quad (9)$$

Russell et al. (2003) used poroelasticity theory (Biot, 1941, and Gassmann, 1951) to equate the  $\lambda$ ,  $\mu$ ,  $\rho$  and  $K$ ,  $\mu$ ,  $\rho$  sets of parameters. Biot (1941) used the Lamé parameters and showed that (Krief et al, 1990)

$$\lambda_{sat} = \lambda_{dry} + \beta^2 M , \quad (10)$$

where  $\lambda_{sat}$  is the 1<sup>st</sup> Lamé parameter for the saturated rock,  $\lambda_{dry}$  is the 1<sup>st</sup> Lamé parameter for the dry frame,  $\beta$  is the Biot coefficient, or the ratio of the volume change in the fluid to the volume change in the formation when hydraulic pressure is constant, and  $M$  is the modulus, or the pressure needed to force water into the formation without changing the volume. Conversely, Gassmann started with the bulk and shear moduli, and derived the following relationship (Krief et al, 1990):

$$K_{sat} = K_{dry} + \beta^2 M , \quad (11)$$

where  $K_{sat}$  is the bulk modulus of the saturated rock,  $K_{dry}$  is the bulk modulus of the dry rock, and  $\beta$  and  $M$  are the same as in equation (10).

By substituting equations (10) and (11) into the two forms of P-wave velocity shown in equation (6), we get

$$V_p = \sqrt{\frac{\lambda_{dry} + 2\mu + \beta^2 M}{\rho_{sat}}} = \sqrt{\frac{K_{dry} + \frac{4}{3}\mu + \beta^2 M}{\rho_{sat}}} = \sqrt{\frac{f + s}{\rho_{sat}}} , \quad (12)$$

where  $f$  is a fluid/porosity term equal to  $\beta^2 M$ , and  $s$  is a dry-skeleton term which can be written either as  $K_{dry} + \frac{4}{3}\mu$  or  $\lambda_{dry} + 2\mu$ .

Note that in equation (12) we have assumed that  $\mu = \mu_{sat} = \mu_{dry}$ , which is a result that can be derived by equating equations (10) and (11). In Russell et al. (2003) this formulation was applied to inverted seismic data, where we estimated the  $P$  and  $S$ -wave impedances,  $Z_p$  and  $Z_s$ . We can extract the terms  $\rho f$  and  $\rho s$  using the following equations:

$$\rho f = I_{Psat}^2 - \gamma_{dry}^2 I_{Ssat}^2 , \quad (13)$$

and

$$s = \gamma_{dry}^2 \mu , \quad (14)$$

$$\text{where } Z_{Psat} = \rho_{sat} V_{Psat}, Z_{Ssat} = \rho_{sat} V_{Ssat}, \gamma_{dry}^2 = \left[ \frac{V_P}{V_S} \right]_{dry}^2 = \frac{\lambda_{dry}}{\mu} + 2 = \frac{K_{dry}}{\mu} + \frac{4}{3} .$$

There are several approaches to estimating  $\gamma_{dry}^2$ . The first is to estimate the dry-rock Poisson's ratio,  $\sigma_{dry}$ , noting that this is given by

$$\sigma_{dry} = \frac{\gamma_{dry}^2 - 2}{2\gamma_{dry}^2 - 2} . \quad (15)$$

Generally, the accepted value of  $\sigma_{dry}$  is in the order of 0.1, which corresponds to a  $V_P/V_S$  ratio of 1.5, or a  $\gamma_{dry}^2$  value of 2.25.

A second approach is to perform laboratory measurements. Murphy et al (1993) measured the  $K_{dry}/\mu$  ratio for clean quartz sandstones over a range of porosities and found that this value was, on average, equal to 0.9. This corresponds to a  $c$  value of 2.233. If the  $K_{dry}/\mu$  value is rounded to 1.0, this implies a  $\sigma_{dry}$  of 0.125, and a corresponding  $\gamma_{dry}^2$  value of 2.333.

Thus, there are a range of values of  $\gamma_{dry}^2$  that depend on the particular reservoir being studied. Table 1 shows a range of these values and the range of their equivalent elastic constant ratios. The value of  $\gamma_{dry}^2$  in this table ranges from a high of 4, meaning that  $\lambda_{dry}/\mu$  is equal to 2, to a low of 1 1/3, meaning that  $K_{dry}/\mu$  is equal to 0.

Note that if  $\gamma_{dry}^2 = 2$ , and we assume that we have inverted for impedances rather than velocities, equations (13) and (14) take the following form:

$$\lambda\rho = Z_{Psat}^2 - 2Z_{Ssat}^2 , \text{ and} \quad (16)$$

$$\mu\rho = Z_{Ssat}^2 \quad (17)$$

Equations (16) and (17) are the LMR (lambda-mu-rho) equations of Goodway et al. (1997).

Table 1. A table of various values of the dry rock  $V_P/V_S$  ratio squared and their relationship to other elastic constants.

$\gamma_{dry}^2$	$(V_p/V_s)_{dry}$	$\sigma_{dry}$	$K_{dry}/\mu$	$\lambda_{dry}/\mu$
4.000	2.000	0.333	2.667	2.000
3.333	1.826	0.286	2.000	1.333
3.000	1.732	0.250	1.667	1.000
2.500	1.581	0.167	1.167	0.500
2.333	1.528	0.125	1.000	0.333
2.250	1.500	0.100	0.917	0.250
2.233	1.494	0.095	0.900	0.233
2.000	1.414	0.000	0.667	0.000
1.333	1.155	-1.000	0.000	-0.667

Using poroelasticity theory we can also generalize the two expressions from Gray et al. (1999). If we start with the Aki-Richards formulation given in equation (1) and use the differential given by

$$\Delta f = \frac{\partial f}{\partial V_p} \Delta V_p + \frac{\partial f}{\partial V_s} \Delta V_s + \frac{\partial f}{\partial \rho} \Delta \rho, \quad (18)$$

we can re-parameterize equation (1) using the parameters  $\gamma_{dry}^2$  and  $\gamma_{sat}^2$ . The final equation is written

$$R_{pp}(\theta) = \left[ \left( 1 - \frac{\gamma_{dry}^2}{\gamma_{sat}^2} \right) \frac{\sec^2 \theta}{4} \right] \frac{\Delta f}{f} + \left[ \frac{\gamma_{dry}^2}{4\gamma_{sat}^2} \sec^2 \theta - \frac{2}{\gamma_{sat}^2} \sin^2 \theta \right] \frac{\Delta \mu}{\mu} + \left[ \frac{1}{2} - \frac{\sec^2 \theta}{4} \right] \frac{\Delta \rho}{\rho} \quad (19)$$

Note that if we let  $\gamma_{dry}^2 = 2$ , equation (19) reduces to the  $\lambda, \mu, \rho$  formulation as given in equation (8). Also, if we let  $\gamma_{dry}^2 = 4/3$ , it reduces to the  $K, \mu, \rho$  formulation given in equation (9). But do these values of 2 and 4/3 make physical sense? As discussed by Russell et al. (2003), these values are not appropriate for typical saturated rocks. If we refer back to Table 1, note that a value of 4/3 implies a dry rock Poisson's ratio of -1 and a value of 2 implies a dry rock Poisson's ratio of 0, neither of which is physically realistic. A value of 2.333, which implies from Table 1 that  $(K/\mu)_{dry} = 1$  and the dry rock Poisson's ratio is 0.125, is more appropriate for rocks such as sandstones. In fact, Dillon et al. (2003) measured  $\gamma_{dry}^2$  values as high as 3 for unconsolidated sandstones in Brazil. We will discuss the results of Dillon et al. (2003) in more detail in the next section.

## FLUID INDICATORS

The theory discussed in the last section leads to the following fluid indicators, which will be compared in the next section:

1. Seismic reflectivities and their combinations, such as fluid factor  $\Delta F$ .
2. The velocity, density and impedance values themselves:  $V_P$ ,  $V_S$ ,  $\rho$ ,  $I_P$  and  $I_S$ , and  $V_P/V_S$  ratio. These values must be derived from seismic data using inversion, but are the measured parameters in Han's dataset.
3. Elastic parameters derived from the velocities and densities, such as bulk modulus ( $K$ ), shear modulus ( $\mu$ , sometimes called  $G$ ), Lamé's parameters ( $\lambda$  and  $\mu$ ) and Poisson's ratio ( $\sigma$ , sometimes called  $\nu$ ). We can also consider ratios and differences of these parameters, such as  $\lambda/\mu$  or  $K \square \mu$ . Also, our key attribute will be the fluid discriminator given by  $\rho f = I_{P\text{sat}}^2 - (V_P/V_S)_{\text{dry}}^2 I_{S\text{sat}}^2$ .

Dillon et al. (2003) performed a multiscale DHI elastic attributes evaluation on 592 rock samples from Tertiary (188) and Cretaceous (404) siliciclastic oil-bearing reservoirs in Brazil. They used most of the attributes that were discussed in our previous section and ranked these methods based on a *fluid indicator coefficient* which diagnoses the sensitivity of the parameter to fluid discrimination. This indicator is defined as the difference between the attribute mean related to each kind of saturation divided by the standard deviation of the attribute related to the oil-saturated reference. As stated by the authors: "This indicator has the advantage of taking into account the spread intrinsic to the attribute value within the universe of samples considered. Higher indicator values represent better discrimination." The authors also used the fluid indicator coefficient to evaluate the best  $c$  value (where  $c = (V_P/V_S)_{\text{dry}}^2$ ) for the generalized fluid method.

Table 2 shows the fluid indicator coefficient analysis for the seven attributes given by:  $I_P - I_S$ ,  $\lambda\rho$ , Poisson's ratio,  $V_P/V_S$  ratio,  $K \square \mu$ ,  $I_P$ , and  $\Delta F$ . Note that lambda-rho ( $\lambda\rho$ ) gives the best discrimination with a value of 7.4, followed by Poisson's ratio and impedance difference both at a value of 6.4.

Table 2. Fluid indicator coefficient analysis for Brazilian Cretaceous and Tertiary sandstones using seven attributes (Dillon et al., 2003).

			$IP - IS$ [m/s kg/m <sup>3</sup> ] × 10 <sup>6</sup>	$\lambda\rho = IP^2 - 2IS^2$ [(m/s kg/m <sup>3</sup> ) <sup>2</sup> ] × 10 <sup>12</sup>	Poisson's ratio [-]	(VP/VS) [-]	$K - G$ [GPa]	$IP$ [m/s. kg/m <sup>3</sup> ] × 10 <sup>6</sup>	Fluid factor [-]
Cretaceous sandstones	water	mean value	4.23	35.0	0.285	1.822	36.9	9.4	0.006
		std. dev.	0.12	1.9	0.007	0.034	2.4	0.3	0.005
	oil	mean value	3.97	30.1	0.268	1.776	35.1	9.1	0.017
		std. dev.	0.12	1.6	0.006	0.017	2.5	0.4	0.004
Fluid indicator coefficient			2.2	3.0	2.8	2.7	0.7	0.8	2.8
Tertiary sandstones	water	mean value	3.26	21.0	0.368	2.183	16.9	6.0	0.008
		std. dev.	0.07	1.0	0.005	0.064	0.6	0.1	0.005
	oil	mean value	2.60	13.4	0.323	1.945	13.5	5.3	0.095
		std. dev.	0.10	1.0	0.007	0.061	0.7	0.2	0.014
Fluid indicator coefficient			6.4	7.4	6.4	3.9	4.8	4.2	6.2

The generalized fluid method of Russell et al. (2003) can be thought of as an “optimized” lambda-rho method, in which the coefficient  $c$  is determined locally for the geology. Table 3, also from Dillon et al. (2003) therefore shows the fluid indicator coefficient as the  $c$  value in the generalized fluid method is changed.

Table 3. Fluid indicator coefficient analysis for Brazilian Cretaceous and Tertiary sandstones using various  $c$  values for the generalized fluid method (Dillon et al., 2003).

		$I_P^2 - cI_S^2$ [(m/s. kg/m <sup>3</sup> ) <sup>2</sup> ] $\times 10^{12}$					
			$c=2.6$	$c=2.7$	$c=2.8$	$c=2.9$	$c=3.0$
Cretaceous sandstones	water	mean value	19.1	16.4	13.8	11.1	8.5
		std. dev.	1.2	1.1	1.2	1.3	1.4
	oil	mean value	14.4	11.8	9.1	6.5	3.9
		std. dev.	0.6	0.7	0.9	1.1	1.3
Fluid indicator coefficient			7.7	6.7	5.4	4.3	3.6
Tertiary sandstones	water	mean value	16.5	15.8	15.0	14.3	13.5
		std. dev.	0.9	0.9	0.8	0.8	0.8
	oil	mean value	9.0	8.2	7.5	6.8	6.0
		std. dev.	1.0	1.0	0.9	0.9	0.9
Fluid indicator coefficient			7.9	7.9	8.0	8.0	8.0
Tertiary + cretaceous sandstones	water	mean value	17.8	16.1	14.0	12.7	11.0
		std. dev.	1.6	1.1	1.2	1.9	2.8
	oil	mean value	11.7	10.0	8.3	6.6	5.0
		std. dev.	2.8	2.0	1.2	1.0	1.5
Fluid indicator coefficient			2.2	3.1	5.0	6.0	3.9

Note from Table 2 that the fluid indicator coefficient now reaches a value of 7.7 for the Cretaceous sandstones and 8 for the Tertiary sandstones. The conclusions reached by Dillon et al. (2003) were as follows:

- 1) In younger, poorly consolidated reservoirs, as the sensitivity to fluids is very good, even the simple acoustic attributes, like the acoustic impedance, are sufficient for a good fluid discrimination.
- 2) In more consolidated reservoirs, common in older sequences, which in this case were represented by the Cretaceous rocks, the combination of the elastic attributes calibrated locally becomes essential for the optimization of the fluid detection process. It can be particularly observed that the indicator suggested by Russell et al.,  $I_P^2 - cI_S^2$ , when used with the correctly calibrated  $c$  value, may be much more efficient than the other attributes.”

In the next section, we will do a similar analysis to that done by Dillon et al. (2003), but using a dataset collected by Han et al. (1985), which will allow us to look at other effects, such as pressure, clay content and porosity.

## APPLICATION TO HAN’S DATASET

Han’s dataset (Han et al., 1985) consists of 75 sandstone samples with porosities from 0 to 30 percent, and the clay content by volume fraction ranging from 0 to 50

percent. Ten samples are tight gas sandstones with very low porosity. Twenty-four samples come from several offshore wells in the Gulf of Mexico, and some of these are poorly consolidated. Eleven samples are from borehole cores which are well-consolidated. Laboratory measurements of P-wave and S-wave velocity, density and porosity were made for these sandstone samples for the dry case and the wet case at the different differential pressures of 5MPa, 10MPa, 20MPa, 30MPa, 40MPa, and 50MPa. Figure 1 shows clay content versus porosity for all samples.

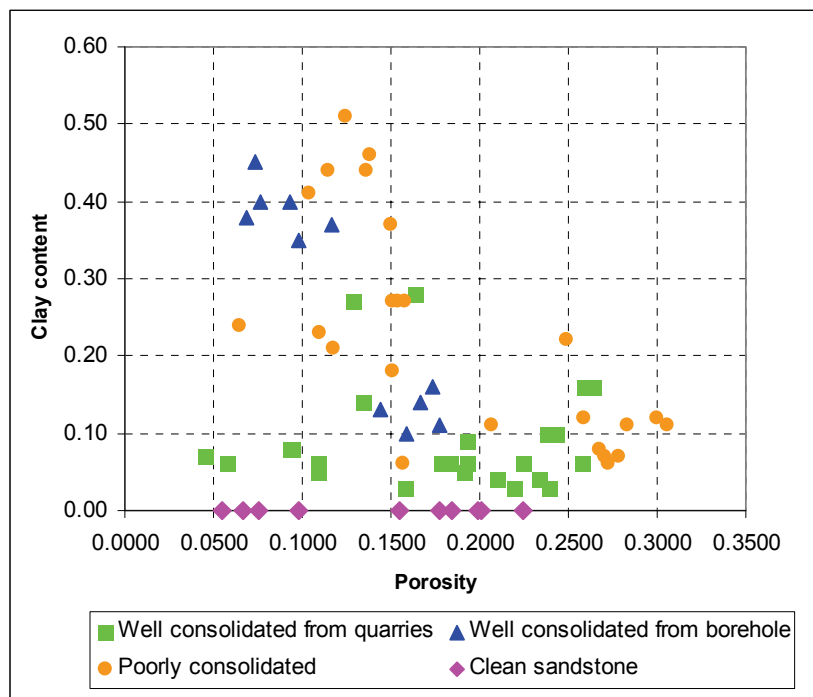


FIG. 1. The range of clay content and porosity for the 75 shaly sandstones of Han's study (Han et al., 1985). Porosity ranges from 2 to 30 percent, and clay content ranges from 0 to about 50 percent.

Due to the range of porosities, clay content and applied pressures found in Han's study, we can thus determine relationships between  $(V_P/V_S)_{dry}^2$  and these three parameters. Figure 2 shows an analysis of  $(V_P/V_S)_{dry}^2$  as a function of porosity for the lowest and highest pressure values of 5 and 50 MPa, using Han's dataset. Note that the velocity ratio goes up as a function of porosity. Figure 3 shows an analysis of  $(V_P/V_S)_{dry}^2$  as a function of clay content for the lowest and highest pressure values of 5 and 50 MPa, using Han's dataset. Note that the velocity ratio goes up slightly for low clay content, but for high clay content shows a decrease.

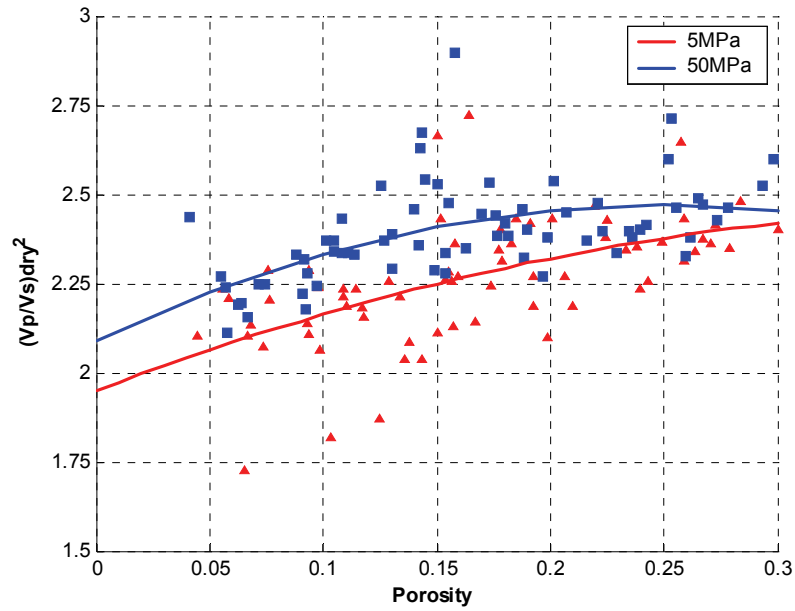


FIG. 2. An analysis of the c value  $(V_p / V_s)_{dry}^2$  as a function of porosity for the lowest and highest pressure values (5 and 50 MPa), using Han's dataset.

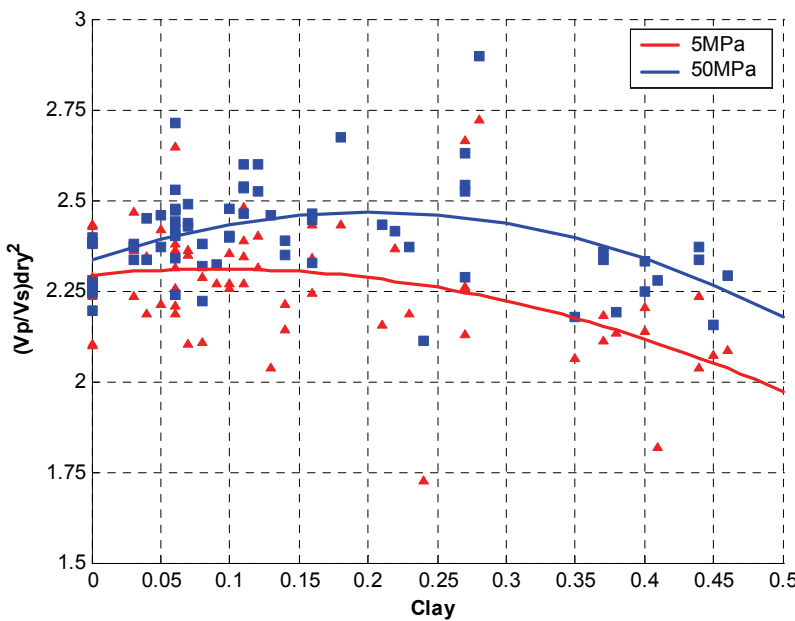


FIG. 3. An analysis of the c value  $(V_p / V_s)_{dry}^2$  as a function of clay content for the lowest and highest pressure values (5 and 50 MPa), using Han's dataset.

Finally, Figure 4 shows an analysis of  $(V_p/V_s)_{dry}^2$  as a function of pressure for all samples using Han's dataset. Note that the velocity ratio goes up as a function of pressure.

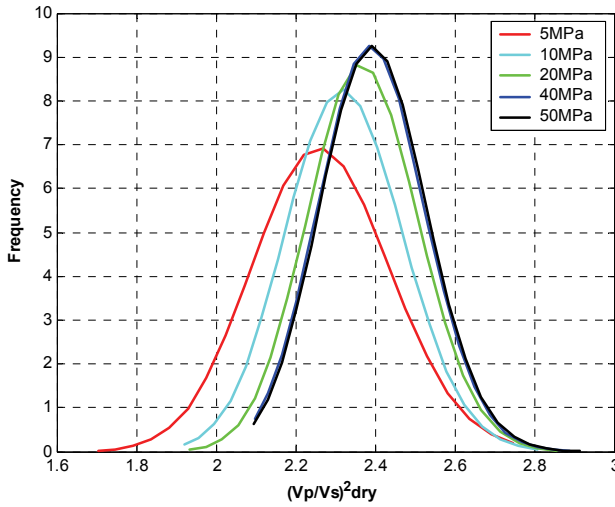


FIG. 4. An analysis of the c value  $(V_p/V_s)_{dry}^2$  as a function of pressure for all samples using Han's dataset.

Now that we have determined accurate values for the dry rock velocity ratio, we can determine which attribute give the best discrimination between the dry and wet samples in Han's study, using Dillon's fluid indicator coefficient. We will start with the shaly sands. Table 4 shows a fluid indicator coefficient analysis for Han's dataset using dry and wet shaly sandstones. Sixteen different attributes have been analyzed. Figure 5 then shows the fluid indicator coefficient analysis for Han's dataset using dry and wet shaly sandstones as a function of pressure, again using sixteen different attributes. In both Table 4 and Figure 5, the best discrimination is found using  $\rho f = I_{Psat}^2 - (V_p/V_s)_{dry}^2 I_{Ssat}^2$ .

Table 4. Fluid indicator coefficient analysis for Han's dataset using dry and wet shaly sandstones, where sixteen different attributes have been analyzed.

Hydrocarbon indicators		Vp (km/s)	Vs (km/s)	Vp/Vs (-)	$\rho$ (g/cc)	I <sub>p</sub> (km/s.g/cc)	I <sub>s</sub> (km/s.g/cc)	u <sub>p</sub> (GPa.g/cc)	$\lambda\rho$ (GPa.g/cc)
Dry	Mean value	3.33	2.22	1.5	2.2	7.4	4.94	26.34	6.29
	Std.dev.	0.73	0.49	0.06	0.2	2.07	1.41	15.74	4.68
Wet	Mean value	3.84	2.19	1.77	2.37	9.15	5.22	29.19	28.59
	Std.dev.	0.6	0.48	0.12	0.13	1.8	1.34	15.76	6.97
Fluid indicator coeffient		0.70	0.06	4.50	0.85	0.85	0.20	0.18	4.76
Hydrocarbon indicators		K (GPa)	u (GPa)	$\lambda$ (GPa)	$u/\lambda$ (-)	$\sigma$ (-)	K-u (GPa)	$I_p^2 \cdot I_s^2$ (GPa.g/cc)	Fluid Factor (-)
Dry	Mean value	10.61	11.62	2.86	0.26	0.1	-1.01	-0.29	-0.29
	Std.dev.	5.5	6.13	2.01	0.17	0.06	1.86	3.85	0.06
Wet	Mean value	20.03	12.11	11.96	1.16	0.26	7.92	21.29	-0.04
	Std.dev.	5.35	6.07	2.42	0.42	0.05	2.6	6.31	0.08
Fluid indicator coeffient		1.71	0.08	4.53	5.29	2.67	4.80	5.61	4.17

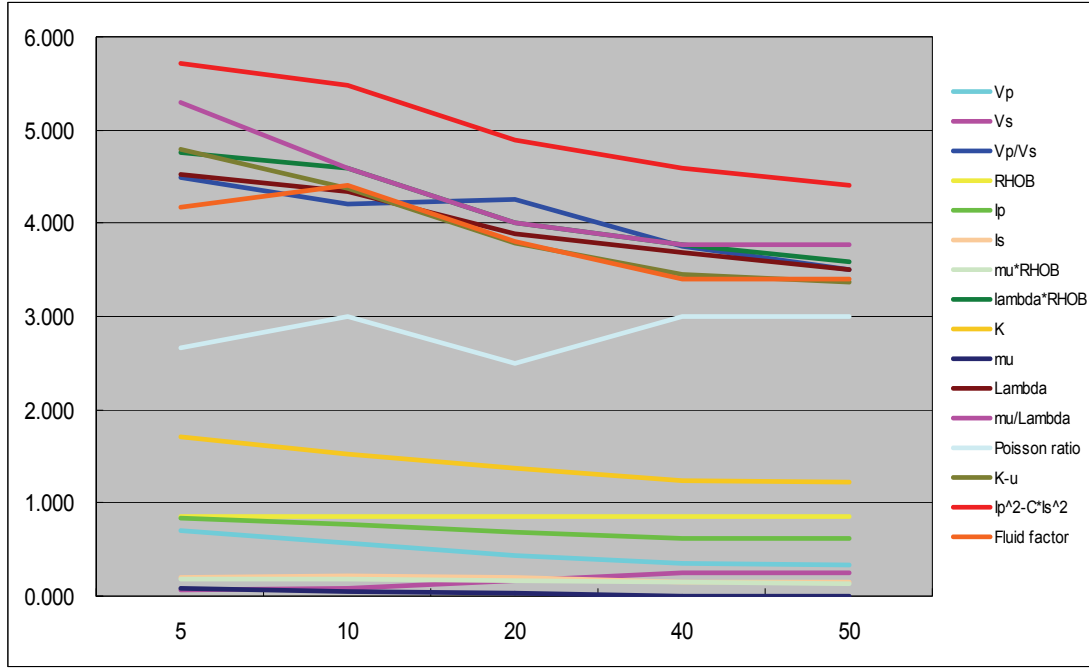


FIG. 5. Fluid indicator coefficient analysis for Han's dataset using dry and wet shaly sandstones, as a function of pressure. Sixteen different attributes have been analyzed.

We will next look at the clean sands. Table 5 shows a fluid indicator coefficient analysis for Han's dataset using dry and wet clean sandstones. Sixteen different attributes have been analyzed. Figure 6 then shows the fluid indicator coefficient analysis for Han's dataset using dry and wet clean sandstones as a function of pressure, again using sixteen different attributes. In both Table 5 and Figure 6, the best discrimination is again found using  $\rho f = I_{Psat}^2 - (V_p / V_s)_{dry}^2 I_{Ssat}^2$ .

Table 5. Fluid indicator coefficient analysis for Han's dataset using dry and wet clean sandstones. Sixteen different attributes have been analyzed.

Hydrocarbon indicators		$V_p$ (km/s)	$V_s$ (km/s)	$V_p/V_s$ (-)	$\rho$ (g/cc)	$I_p$ (km/s.g/cc)	$I_s$ (km/s.g/cc)	$\frac{u\rho}{I_p}$ (GPa.g/cc)	$\lambda\rho$ (GPa.g/cc)
5MPa	Dry	Mean value	4.39	2.91	1.51	2.26	10.01	6.63	46.07
	Dry	Std.dev.	0.66	0.46	0.04	0.17	2.18	1.52	21
	Wet	Mean value	4.71	2.95	1.61	2.41	11.4	7.13	52.47
	Wet	Std.dev.	0.56	0.44	0.06	0.1	1.85	1.36	20.02
Fluid indicator coeffient		0.48	0.09	2.50	0.88	0.64	0.33	0.30	2.95
Hydrocarbon indicators		$K$ (GPa)	$u$ (GPa)	$\lambda$ (GPa)	$u/\lambda$ (-)	$\sigma$ (-)	$K-u$ (GPa)	$I_p^2-cI_s^2$ (GPa.g/cc)	Fluid Factor (-)
5MPa	Dry	Mean value	18.71	19.9	5.45	0.29	0.11	-1.19	0.89
	Dry	Std.dev.	6.51	7.73	2.14	0.13	0.04	2.37	4.57
	Wet	Mean value	25.94	21.53	11.58	0.59	0.18	4.41	14.87
	Wet	Std.dev.	5.88	7.33	2.08	0.19	0.04	2.67	5.53
Fluid indicator coeffient		1.11	0.21	2.86	2.31	1.75	2.36	3.06	2.00

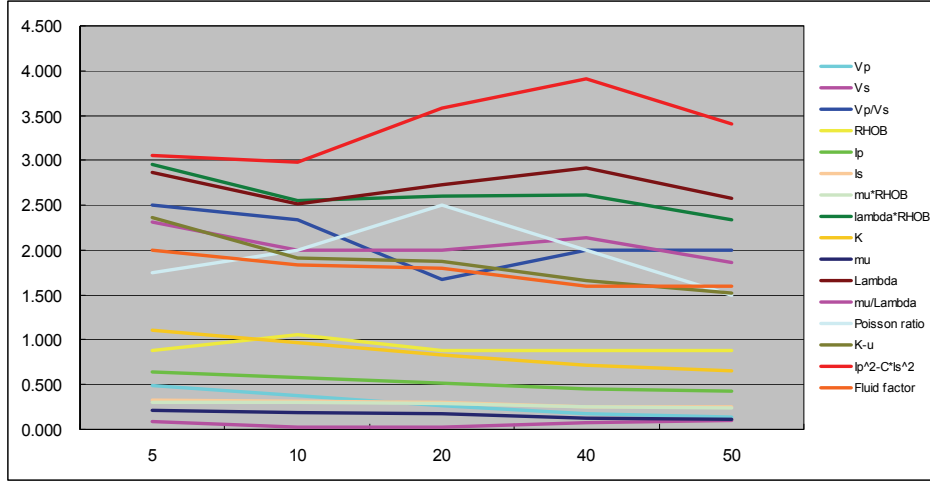


FIG. 6. Fluid indicator coefficient analysis for Han's dataset using dry and wet clean sandstones, as a function of pressure. Sixteen different attributes have been analyzed.

## CONCLUSIONS

This has been an empirical study of various fluid indicators, using the extensive core dataset measured by Han et al. (1985). By analyzing these measurements, we were able to determine relationships between the dry rock  $V_P$  to  $V_S$  ratio as a function of porosity, clay content and pressure. This ratio is a key parameter in the generalized fluid method of Russell et al. (2003). In general, we found that the ratio went up as a function of porosity and pressure, but down as a function of clay content. Using these computed velocity ratios, we were then able to compare the generalized fluid method against other methods of fluid discrimination. To evaluate their effectiveness, we used the fluid indicator coefficient as described by Dillon et al. (2003). In all cases, we found that the generalized fluid method gave the best fluid discrimination. We also reviewed the results given by Dillon et al. (2003) for measured cores from Brazil. Our analysis confirmed their observation that the value of dry rock velocity ratio used in the generalized fluid method goes up as a function of depth in the more consolidated reservoirs (since pressure and depth are related).

However, we did not analyze real data in this study, and Dillon et al. (2003) also make the following statement in their paper: "At the seismic scale, however, this same attribute (i.e. the generalized fluid method) does not perform as predicted in the rock (plug) scale, due to the deterioration of the signal-to-noise ratio inherent to the operations involved in its calculation. In this context, the DHI attribute given by  $I_P - I_S$  presents the advantages of: (1) having, approximately, the same discriminatory power of  $\lambda\rho$  (where  $I_P^2 - 2I_S^2 = \lambda\rho$ ), since these two parameters are almost linearly related and (2) being simpler to calculate and not subject to such a strong degeneration of the signal-to-noise ratio as  $\lambda\rho$  or, generically,  $I_P^2 - cI_S^2$ ."

As an answer to this, we suggest that the parameters extracted using the generalized fluid term extraction (Russell et al., 2006), which again is crucially dependent on the dry rock velocity ratio, is probably a better method to use, since it

does not involve the squaring of the data volumes. However, this is something to be determined in a future study.

### **ACKNOWLEDGEMENTS**

We wish to thank our colleagues at the CREWES Project and CGGVeritas for their support and ideas, as well as the sponsors of the CREWES Project.

### **REFERENCES**

- Aki, K., and Richards, P.G., 1980, Quantitative seismology: Theory and methods: W. H. Freeman and Co.
- Biot, M.A., 1941, General theory of three-dimensional consolidation: Journal of Applied Physics, **12**, 155-164.
- Dillon, L., Schwedersky, G., Vasquez, G., Velloso, R., and Nunes, C., 2003, A multiscale DHI elastic attributes evaluation: The Leading Edge, **22**, no. 10, 1024-1029.
- Fatti, J. L., Vail, P. J., Smith, G. C., Strauss, P. J., and Levitt, P. R., 1994, Detection of gas in sandstone reservoirs using AVO analysis: A 3-D seismic case history using the geostack technique: Geophysics, **59**, 1362-1376.
- Gassmann, F., 1951, Über die Elastizität poröser Medien, Vierteljahrsschrift der Naturforschenden Gesellschaft in Zürich, **96**, 1-23.
- Goodway, W., Chen, T., and Downton, J., 1997, Improved AVO fluid detection and lithology discrimination using Lamé petrophysical Parameters; “Lambda-Rho”, “Mu-Rho”, & “Lambda/Mu fluid stack”, from P and S inversions.
- Gray, D., Goodway, W., and Chen, T., 1999, Bridging the gap: Using AVO to detect changes in fundamental elastic constants: 1999 SEG meeting abstracts, 852-855.
- Han, D.H., Nur, A., and Morgan, S., 1985, Effects of porosity and clay content on wave velocities in sandstones: Geophysics, **51**, 2093-2107.
- Krief, M., Garat, J., Stellingwerff, J. and Ventre, J., 1990, A petrophysical interpretation using the velocities of P and S waves: The Log Analyst, Nov-Dec, 355-369.
- Murphy, W., Reischer, A., and Hsu, K., 1993. Modulus Decomposition of Compressional and Shear Velocities in Sand Bodies: Geophysics **58**, 227-239
- Russell, B.H., Gray, D., Hampson D.P., and Lines, L.R., 2006, Linearized AVO and poroelasticity: CREWES Research Report — Volume 18 (2006)
- Russell, B.H., Hedlin, K., Hilterman, F.J., and Lines, L.R., 2003, Fluid-property discrimination with AVO: A Biot-Gassmann perspective: Geophysics, **68**, 29-39.
- Shuey, R.T., 1985, A simplification of the Zoeppritz equations: Geophysics, **50**, 609-614.